The role of Trivelpiece–Gould waves in antenna coupling to helicon waves

Donald Arnush

Electrical Engineering Department, University of California, Los Angeles, California 90095-1594

It is well known that the simple theory of helicon waves, in which the electron mass m_e is neglected, is valid only if E_z also vanishes, a condition which is not satisfied in experiment. Exact solutions of cold plasma theory with finite m_e and E_z predict the existence of additional highly damped Trivelpiece–Gould (TG) modes (H-TG theory), which can greatly modify the nature of helicon discharges. However, most experiments have been explained using only the simple theory for which the helicon waves are undamped. In that case, antenna-plasma-coupling calculations predict infinite resonances. To avoid this problem theorists have set $E_z = 0$ and included finite m_e effects (the TE-H theory). By comparing the TE-H theory with exact (i.e., closed form) solutions for uniform density, the role of TG modes has been clarified. To do so for nonuniform density, a new algorithm is developed to treat the case of high magnetic fields, when the wave equation becomes singular. The results show that, though the wave patterns are not greatly affected by TG modes except at low magnetic fields or near the radial boundary, the k_z spectrum and radial profile of the energy deposition are greatly modified. In particular, the peaks in the TE-H-mode spectrum, which lead to predictions of erroneously high antenna loading, are suppressed and broadened by the TG modes which also produce high edge absorption. Both the TE-H and exact theories give maximum antenna loading for $\frac{1}{2}m_e(\omega/k)^2 \approx 10$– $100\,\mathrm{eV}$, in contrast to several hundred electron volts predicted by the simple theory. © *2000 American Institute of Physics.* [S1070-664X(00)01607-4]

I. INTRODUCTION

Plasma sources employing helicon wave excitation are of current interest because they may provide the high density and uniformity needed for the fabrication of the next generation of semiconductor circuits.[1,2] It has been known for some time[3] that finite electron mass m_e, couples helicon to electron cyclotron Trivelpiece–Gould (TG) waves[4–6] in uniform plasma. Despite that fact, most early experiments were interpreted using a simple model of helicon waves in which m_e, and hence $\delta = \omega/\omega_c$ is neglected.[7–11] More recently Shamrai *et al.*[12–14] have investigated antenna coupling to a uniform density plasma and explained why, for most cases of interest, the wave magnetic fields, which are the easiest to measure, are dominated by the helicon waves. They also showed that the major channel for plasma heating is coupling to helicon waves, which are weakly damped throughout the body of the plasma, and ''mode conversion'' from helicon to TG waves near the surface. The TG waves are strongly damped. Kamenski and Borg[15] treated antenna coupling to nonuniform plasma theoretically, assuming that the axial electric field vanishes, and neglected TG waves. More recently, Arnush and Chen[16,17] have calculated antenna coupling to a nonuniform plasma at low to moderate static magnetic field ($B_0 \lesssim 1\,\mathrm{kG}$) and density ($n_0 \lesssim 10^{13}\,\mathrm{cm}^{-3}$), to first order in δ, and found results in agreement with Shamrai *et al.* for nearly uniform density profiles. For more centrally peaked profiles (e.g., for a parabola) they found that the large radial TG currents near the surface are canceled by helicon currents and consequently the plasma center is more intensely heated. In contrast to the prior studies of cylindrically bounded plasmas, Borg and Boswell[18] considered wave excitation by an infinite line source in infinite uniform collisionless plasma. They found that the TG mode does not lead to a significant increase in antenna coupling, and that the resonance cone is not a location of spatially resonant power flux.

In this paper the antenna coupling to cylindrically symmetric plasma is considered using a collisional cold plasma dielectric. The role of TG wave damping is explicitly explored by comparing uniform density, exact solutions with solutions using a transverse electric (TE) approximation that includes only helicon waves (TE-H), similar to that investigated by Kamenski and Borg. For nonuniform densities and low to moderate magnetic fields ($B_0 \lesssim 300\,\mathrm{G}$ for a 5 cm radius plasma) the plasma field equations can be solved numerically by standard methods. At higher magnetic fields the equations are singular (i.e., the coefficient of the highest order derivative tends to zero with increasing B_0) and an approximate solution is obtained and investigated. The main focus of this paper is a discussion of the dependence on density and magnetic field of the power spectrum of waves absorbed by the plasma, the radial distribution of the power absorbed, and the antenna resistance. These quantities are featured primarily because their understanding is key to designing optimal helicon sources, and also because the presence of TG waves has a relatively small effect on the spatial dependence of the observed magnetic wave fields making it difficult to measure.

II. GENERAL FORMULATION

A. Boundary conditions

Consider a cylindrical plasma of radius a, which is uniform axially and nonuniform radially, and which is enclosed

3042

in a conducting cylinder of radius c, with an intervening thin shell antenna of radius b, such that $a<b<c$. There are two linearly independent sets of solutions that are finite on the axis. These plasma ''basis functions'' are distinguished by their behavior near the axis and are denoted by lower case symbols ($\mathbf{e}$, $\mathbf{b}$, and $\mathbf{j}$ for $\mathbf{E}$, $\mathbf{B}$, and $\mathbf{J}$) and the subscripts 1 and 2 (for a uniform plasma 1 denotes the helicon and 2 the TG wave). Take the Fourier transform of each component $\underline{V}_i$, of any wave quantity to be

$$V_i(r,m,k)=\int_{-\infty}^{\infty}dz\int_0^{2\pi}\frac{d\phi}{2\pi}\underline{V}_i(r,\phi,z)e^{-i(m\phi+kz)}. \quad (2.1)$$

Variables are underlined to distinguish configuration-space from k-space functions. In Eq. (2.1) and the following we use $k\equiv k_z$. There are ten unknown basis function coefficients (2 vacuum regions $\times 2$ polarizations $\times 2$ behaviors at 0 and infinity +2 plasma basis function sets). Using the usual ten boundary conditions ($\mathbf{E}_{\text{tan}}=0$ at $r=c$, is continuous at $r=b$ and $r=a$; $\mathbf{B}_{\text{tan}}$ is continuous at $r=a$ but undergoes a jump at $r=b$) and the fact that in the vacuum spaces we have

$$E_\phi=\frac{mk}{rT_0^2}E_z+i\frac{\omega}{T_0^2}\frac{\partial}{\partial r}B_z, \quad B_\phi=\frac{mk}{rT_0^2}B_z-i\frac{\omega}{T_0^2}\frac{\partial}{\partial r}E_z, \quad (2.2)$$

where $T_0=\sqrt{k^2-k_0^2}$ is the transverse wave number in the vacuum and $k_0=\omega/c$, Arnush and Chen[17] have shown that $V_i(r)$ can expressed as

$$V_i(r)=\frac{H_2 v_{1,i}(r)-H_1 v_{2,i}(r)}{F_1 G_2-F_2 G_1}i\mu_0 K_\phi. \quad (2.3)$$

The m and k functionality is understood. K_ϕ is derived from the antenna current density of the form $\underline{\mathbf{J}}(r,\phi,z)=\delta(r-b)\underline{\mathbf{K}}(\phi,z)$ [the surface current is assumed to be closed so that $(m/b)K_\phi+kK_z=0$] and

$$F_n=b_{n,r}(a)+\frac{k}{T_0}p_m(a)\tilde{b}_{n,z}(a)+\frac{m}{aT_0^2}\mu_0[\omega\epsilon_0 e_{n,z}(a)], \quad (2.4a)$$

$$G_n=j_{n,r}(a)+\frac{m}{a}\frac{k_0^2}{T_0^2}\frac{1}{\mu_0}\tilde{b}_{n,z}(a)$$
$$+\omega\epsilon_0\left[\frac{k}{T_0}q_m e_{n,z}(a)-\tilde{e}_{n,r}(a)\right], \quad (2.4b)$$

$$H_n=\frac{kb}{T_0 a}p_m(b)\mu_0 G_n-\frac{m}{a}\frac{k_0^2}{T_0^2}\rho_m F_n, \quad (2.4c)$$

where

$$p_m(r)=\frac{K'_m(T_0 r)I'_m(Tc)-K'_m(T_0 c)I'_m(T_0 r)}{K_m(T_0 a)I'_m(T_0 c)-K'_m(T_0 c)I_m(T_0 a)}, \quad (2.5a)$$

$$q_m=\frac{K'_m(T_0 a)I_m(T_0 c)-K_m(T_0 c)I'_m(T_0 a)}{K_m(T_0 a)I_m(T_0 c)-K_m(T_0 c)I_m(T_0 a)}, \quad (2.5b)$$

$$\rho_m=\frac{K_m(T_0 b)I_m(T_0 c)-K_m(T_0 c)I_m(T_0 b)}{K_m(T_0 a)I_m(T_0 c)-K_m(T_0 c)I_m(T_0 a)}. \quad (2.5c)$$

Equations (2.4), (2.5), and the forthcoming text are somewhat simplified from Arnush and Chen[17] by the use of $\tilde{b}_r=ib_r$, $\tilde{b}_\phi=ib_\phi$, and $\tilde{e}_r=ie_r$. Note that the term $\tilde{e}_{n,r}$ in the expression for G_n was inadvertently omitted in the original published version of this equation.

B. Wave equations

Using the Krook-modified dielectric tensor $\mathbf{K}=\boldsymbol{\epsilon}/\epsilon_0$, including electron–ion and electron–neutral collisions and the notation of Stix:[19] $\epsilon_{xx}=\epsilon_{yy}=S$, $\epsilon_{zz}=P$, and $\epsilon_{yx}=-\epsilon_{xy}=iD$, the equations for the wave fields are

$$\frac{\partial}{\partial r}E_\phi=\frac{m}{r}\tilde{E}_r-\frac{1}{r}E_\phi+k_0 c\tilde{B}_z, \quad (2.6a)$$

$$\frac{\partial}{\partial r}E_z=k\tilde{E}_r-k_0 c\tilde{B}_\phi, \quad (2.6b)$$

$$\frac{\partial}{\partial r}\tilde{B}_\phi=\frac{m}{r}\frac{k}{k_0}\frac{1}{c}E_\phi-\frac{1}{r}\tilde{B}_\phi+k_0\left(P-\frac{m^2}{k_0^2 r^2}\right)\frac{1}{c}E_z, \quad (2.6c)$$

$$\frac{\partial}{\partial r}\tilde{B}_z=-D\frac{k_0}{c}\tilde{E}_r+(k^2-k_0^2 S)\frac{1}{k_0 c}E_\phi+\frac{m}{r}\frac{k}{k_0 c}E_z, \quad (2.6d)$$

$$B_r=\frac{1}{k_0 c}\left(\frac{m}{r}E_z-kE_\phi\right), \quad (2.6e)$$

$$\tilde{E}_r=-\frac{D}{S}E_\phi+\frac{kc}{k_0 S}\tilde{B}_\phi-\frac{m}{r}\frac{c}{k_0 S}\tilde{B}_z. \quad (2.6f)$$

Equations (2.6a)–(2.6d) form a closed set and can be solved numerically by standard methods except at large magnetic fields. If the density is uniform the basis function fields are the familiar Bessel function solutions given by

$$b_{n,z}(r)=J_m(T_n r), \quad (2.7a)$$

where

$$ST_n^4+T_n^2[k^2(S+P)-k_0^2(SP+RL)]$$
$$-P(k_0^2 R-k^2)(k^2-k_0^2 L)=0, \quad (2.7b)$$

$$R,L=(S\pm D)/2. \quad (2.7c)$$

III. SPECIFIC SOLUTIONS

A. Transverse electric helicon solution (TE-H)

If we assume that $E_z\equiv 0$ in the plasma, then only the TE mode exists in the cavity. Including the single, helicon, plasma mode there are five basis functions and hence five unknown coefficients. Three of the general boundary conditions are automatically satisfied so that there are seven boundary conditions, and the system of equations for the coefficients is overdetermined. We derive the TE-H analog of Eq. (2.3) without the use of the boundary conditions on B_ϕ The consequences of this action are discussed in Sec. III C. The results are

$$\mathbf{V}(r)=\frac{\mathbf{v}(r)}{F^{(0)}}\left(i\frac{kb}{T_0 a}p(b)\mu_0 K_\phi\right), \quad (3.1a)$$

$$F^{(0)} = b_r(a) + \frac{k}{T_0} p(a) \tilde{b}_z(a). \tag{3.1b}$$

A TE-H resonance as a function of k therefore occurs for $F^{(0)} = 0$, in contrast to the simple theory condition[7] $b_r(a) = 0$.

If we set $E_z \equiv 0$ in Eq. (2.6) the second equation becomes algebraic and the set is overdetermined. However, we note that in the limit $m_e \to 0$, $P \propto m_e^{-1}$ and $E_z \propto m_e$. Consequently, the product $P E_z$ in Eq. (2.6c), and hence the equation is indeterminate. We therefore eliminate the equation from the set and obtain the following:

$$\frac{\partial}{\partial r} E_\phi = k_0 \left(1 + \frac{m^2}{r^2(k^2 - k_0^2 S)} \right) c \tilde{B}_z$$
$$+ \frac{1}{r} \left(m \frac{k_0^2 D}{k^2 - k_0^2 S} - 1 \right) E_\phi, \tag{3.2a}$$

$$\frac{\partial}{\partial r} \tilde{B}_z = -\frac{m}{r} \frac{k_0^2 D}{k^2 - k_0^2 S} \tilde{B}_z - \frac{1}{ck_0} T_3^2 E_\phi, \tag{3.2b}$$

$$\tilde{B}_\phi = \frac{kk_0}{k^2 - k_0^2 S} \left(\frac{D}{c} E_\phi + \frac{m}{k_0 r} \tilde{B}_z \right), \tag{3.2c}$$

$$B_r = -\frac{k}{ck_0} E_\phi, \tag{3.2d}$$

$$\tilde{E}_r = \frac{k_0^2}{k^2 - k_0^2 S} \left(D E_\phi + \frac{m}{k_0 r} c \tilde{B}_z \right). \tag{3.2e}$$

In Eq. (3.2) we have used

$$T_3^2 = \frac{(k_0^2 R - k^2)(k^2 - k_0^2 L)}{k^2 - k_0^2 S}. \tag{3.3}$$

For a uniform plasma the solution to Eq. (3.2) is $b_z(r) = J_m(T_3 r)$. T_3 can be obtained from Eq. (2.7) by taking the limit $P \to \infty$ and self-consistently neglecting T^4. Note that this solution differs from the $m_e \to 0$ limit since in that case $S = 0$, D is real, and hence T_3 is real. Consequently, the resonances of Eq. (3.1) are infinite. The inclusion of these first-order terms provides dissipation which limits and broadens the resonance. In addition, T_3 is a good approximation to the helicon root of Eq. (2.7), except at long wavelengths well above the cutoff for helicon wave propagation. For nonuniform plasma, the closed set of Eqs. (3.2a) and (3.2b) are solved as in the general case.

B. Helicon Trivelpiece–Gould solution (H-TG)

If the density is uniform the closed form Bessel solutions are used. If the density is nonuniform, and B_0 is not too large (typically $B_0 < 300\,\text{G}$) the solutions of (2.7) are used in the first radial step from the axis and Eq. (2.6) is integrated outward to the plasma surface. If B_0 is sufficiently large the equation set (2.6) becomes numerically difficult to solve and we resort to solving it using a series in m_e.

If we integrate Eq. (2.6) starting near the axis, each basis function will be a linear combination of TG-like and helicon-like waves. At large magnetic fields the TG radial wave number can be approximated by $T_2^2 \cong -k^2 P/S$. If $|\text{Im } T_2 a| \gg 1$ both solutions are dominated by the TG-like functions, then Eq. (2.3) requires the calculation of a small difference of large numbers. To avoid the difficulties inherent in that process note that any two linearly independent solutions of Eq. (2.6) may be used in Eq. (2.3). We therefore choose the solutions to Eq. (3.2) for the first, helicon-like basis functions. The second, TG-like solution is obtained by an expansion in m_e. For m_e of order ϵ, S and P are of order ϵ and ϵ^{-1}, respectively, in the limit $\epsilon \to 0$. We expand the field components in the following series:

$$V_i = \exp\left(i \frac{\psi}{\epsilon} \right) \sum_{n=0}^{\infty} A_{i,n} \epsilon^n. \tag{3.4}$$

If we require a nonzero solution and calculate to order ϵ^0 we obtain

$$\psi' = \frac{\partial \psi}{\partial r} = k \sqrt{\frac{-P}{S}}, \quad \beta = \frac{D}{(-PSr^2)^{1/4}}, \tag{3.5a}$$

$$\Psi(k,r) = -i \int_r^a dr' \left[\psi' + \frac{k_0^2 (PS - D^2) + \frac{m}{r'} \frac{\partial D}{\partial r'}}{2k\sqrt{-PS}} \right], \tag{3.5b}$$

$$b_{2,r} = 0, \quad \tilde{b}_{2,z} = \frac{\beta(r)}{\beta(a)} \exp(\Psi(k,r)), \quad b_{2,\phi} = -\frac{iS}{kD} \tilde{b}_{2,z}, \tag{3.5c}$$

$$(\tilde{e}_{2,r}, e_{2,\phi}, e_{2,z}) = -\frac{c}{k_0 D} \left(-i\psi', -\frac{m}{r}, -k \right) \tilde{b}_{2,z}. \tag{3.5d}$$

C. Relationship of the solutions

Neglecting terms of order $(k_0/T_0)^2$, as well as the displacement current terms (in square brackets) in Eq. (2.4), Eq. (2.3) becomes

$$\mathbf{V}(r) = \frac{j_{2,r}(a)\mathbf{v}_1(r) - j_{1,r}(a)\mathbf{v}_2(r)}{j_{2,r}(a)F_1^{(0)} - j_{1,r}(a)F_2^{(0)}} \left(i \frac{kb}{T_0 a} p(b) \mu_0 K_\phi \right), \tag{3.6}$$

which is valid provided that the outer cylinder-plasma gap, c-a, is not too small.[17] Resonance occurs as a function of k if the denominator of Eq. (3.6) vanishes. Antiresonances occur if either one of the basis function radial currents vanishes.[20] Thus, if for a given k, $j_{1,r}(a) = 0$ (equivalent to the simple helicon boundary condition for uniform plasma), only helicon waves are present and we recover Eq. (3.1). However, except for rare coincidences, the amplitude of the helicon wave is reduced since $F_1^{(0)}$ will not be near zero at that k. For high magnetic fields ($\delta = \omega/\omega_{ce} \ll 1$), $\text{Im}\{T_2\}$ (T_1 and T_2 are the helicon and TG radial wave numbers) is very large and the second term in the numerator of Eq. (3.6) is negligible compared to the first except near the surface. Similarly, since $\mu_0 j_{i,r} \cong T_i b_{i,r}$ (the relationship is exact for a uniform density) the magnitude of the ratio of the second to the first term in the denominator is of the order of $|T_1/T_2| \ll 1$. Thus, neglecting the second terms in the ratio, Eq. (3.1) is recovered from Eq. (3.6) in the helicon approximation.

However, in calculating the configuration space fields from these equations by taking the Fourier transform, the results are dominated by resonances due to the vanishing of the real part of $F_1^{(0)}$. The imaginary part of this quantity, related to the imaginary part of T_1, is very small since the helicon wave is undamped to lowest order in m_e. On the other hand, the imaginary part of $F_2^{(0)}$ is significant since the TG wave is heavily damped. Thus, to meet the boundary conditions, both helicon and TG waves must be induced at the plasma surface. The TG waves reduce and broaden the resonance and significantly modify the power coupling.

Consider now the consequences of ignoring the boundary conditions on the magnetic field in deriving Eq. (3.1). Using ΔB_ϕ^A as the value of B_ϕ just outside the antenna, minus that just inside, the jump condition across the antenna is satisfied if the following quantity vanishes:

$$\Delta B_\phi^A - \mu_0 K_z = \frac{k_0^2}{T_0^2} \mu_0 K_\phi. \tag{3.7}$$

Since, for most cases of interest, $(k_0/T)^2$ is very small, the jump condition is satisfied in the sense that the correction is much smaller than any of the individual terms in the equation. Defining the difference in B_ϕ at the plasma boundary as ΔB_ϕ^P in a similar fashion, we obtain

$$\Delta B_\phi^P = -i \frac{k}{T_0^2} \mu_0 j_r(a). \tag{3.8}$$

The simple theory was derived for uniform plasma where j_r is proportional to b_r. The simple boundary condition therefore is equivalent to setting ΔB_ϕ^P, and hence the radial current, equal to zero. In the general theory we set $\Delta B_\phi^P = 0$ and an axial current carried by the TG waves balances the radial current near the surface. In the TE-H theory, since the radial current is not necessarily equal to zero it must be balanced by an *ad hoc* axial surface current given through Ampere's law by $\Delta B_z^P = \mu_0 K_z(a)$.

IV. ANALYSIS

A. Measures of power coupling

We define the specific plasma power spectral function, $S_P(k')$ as the power absorbed by the plasma for an antenna with $K_\phi = \delta(k - k')$,

$$S_P(k') = \frac{1}{2} \mathrm{Re}\left\{ \int \mathbf{E}^* \cdot \mathbf{J}_{plasma} d^3r \right\}. \tag{4.1}$$

Since $S_P(k')$ is an even function, for 1 A the plasma power spectral function $P_P(k)$, and plasma resistance R_P, is

$$P_P(k) = S_P(k) p_A(k)$$

$$= \frac{\omega \epsilon_0}{2} \int_0^a \mathrm{Im}\{S(|\tilde{E}_r|^2 + |E_\phi|^2) + P|E_z|^2$$

$$+ 2D \, \mathrm{Re}\{\tilde{E}_r^* E_\phi\}\} r \, dr, \tag{4.2a}$$

$$R_P = 2 \int_0^\infty P_P(k) dk, \tag{4.2b}$$

where

$$p_A(k) = |K_\phi(k)|^2 + |K_\phi(-k)|^2. \tag{4.2c}$$

There has been considerable speculation in the literature about helicon waves accelerating electrons with the velocity ω/k by the Landau damping mechanism. It is therefore useful to express $P_p(k)$ as a function of the energy of the electrons $u = \frac{1}{2} m_e (\omega/k)^2$ using a variable transformation, as follows:

$$P_u(u) = \sqrt{\frac{m_e \omega^2}{8u^3}} P_k\left(\sqrt{\frac{m_e \omega^2}{2u}} \right), \tag{4.3a}$$

$$R_P = 2 \int_0^\infty P_u(u) du. \tag{4.3b}$$

Similar to $P_P(k)$, the antenna power spectral function $P_A(k)$, and antenna loading resistance R_A, can be defined as

$$P_A(k) = -\frac{1}{2} \mathrm{Re}\left\{ \int \mathbf{E}^* \cdot \mathbf{J}_{antenna} d^3r \right\}$$

$$= \frac{\mu_0 c}{2} \frac{k_0 a}{T_0} p_A(k) \mathrm{Im}\left\{ p_m(b) \frac{\tilde{B}_z}{K_\phi} \right.$$

$$\left. + \frac{m}{ka} \frac{k_0}{cT_0} \rho_m \frac{E_z}{K_\phi} \right\}\Bigg|_{r=a} \tag{4.4a}$$

$$R_A = 2 \int_0^\infty P_A(k) dk. \tag{4.4b}$$

Note that for most cases of interest the second term in the expression for $P_A(k)$ is negligible and hence P_A is proportional to the surface axial magnetic wave field. As we shall see, at high magnetic fields the spectrum is dominated by one or a few resonances and the antenna resistance may be estimated from the sum of the residues at the resonances. If no power escapes axially (due to either end reflections or total absorption in a very long cylinder) then

$$P_A(k) = P_P(k), \quad R_A = R_P. \tag{4.5}$$

Indeed, the degree to which these equalities are met is a good measure of accuracy of basis functions either numerically integrated or approximated. It is also instructive to consider $P_r(r)$, the power absorbed in a differentially thin radial shell the length of the cylinder

$$P_r(r) = \frac{\omega \epsilon_0}{2} \int_{-\infty}^\infty \mathrm{Im}\{S(|\tilde{E}_r|^2 + |E_\phi|^2) + P|E_z|^2$$

$$+ 2D \, \mathrm{Re}\{\tilde{E}_r^* E_\phi\}\} dk, \tag{4.6a}$$

$$R_P = 2 \int_0^a P_r(r) r \, dr. \tag{4.6b}$$

To illustrate the results of this formulation the following parameters were selected for argon, using a collision frequency calculated from the electron–ion analytic form and the electron–neutral cross section[21] convolved with a Maxwellian electron distribution:

$$a = 5 \text{ cm}, \quad b = 5.5 \text{ cm}, \quad c = 15 \text{ cm},$$

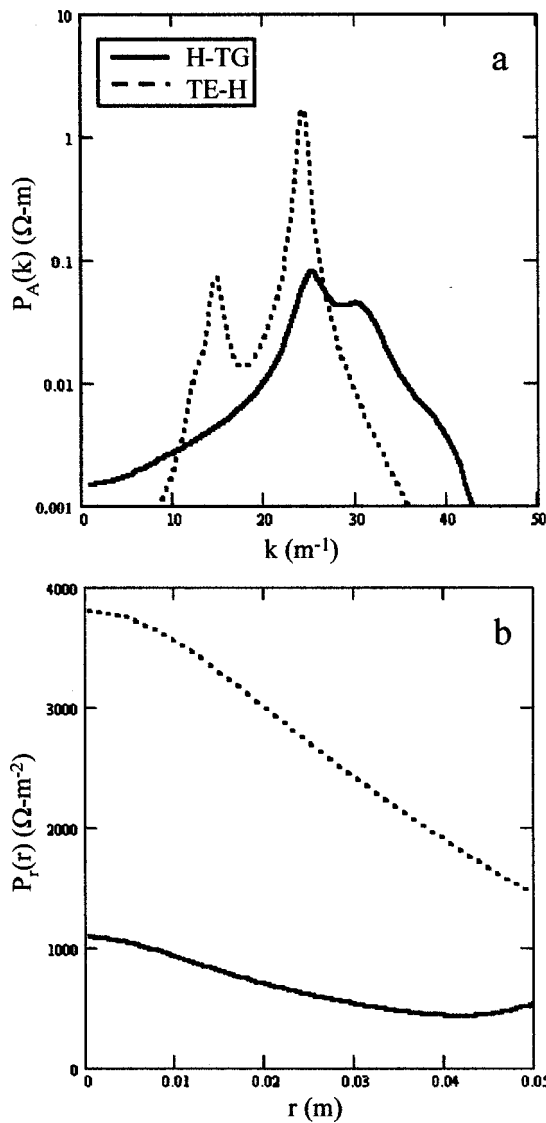$$f_0 = 13.56 \text{ MHz}, \quad T_e = 3 \text{ eV}, \quad P_0 = 3 \text{ mTorr}. \tag{4.7}$$

FIG. 1. H-TG vs TE-H power absorption spectrum (a), and radial profile (b), for a uniform density $n_0 = 10^{11}$ cm^{-3} and magnetic field $B_0 = 25$ G.

FIG. 2. H-TG vs TE-H power absorption spectrum (a), and radial profile (b), for a uniform density $n_0 = 10^{12}$ cm^{-3} and magnetic field $B_0 = 100$ G.

A half-turn helicon antenna is used, and results are quoted for the $m = 1$ azimuthal Fourier component. Bessel functions of a complex argument, $J_m(z)$, are calculated using a power series for $|z| < 11$ and an asymptotic series[22] for $|z| \geqslant 11$. For a radially nonuniform density, for each k, Eq. (2.6) is integrated if Re$\{\Psi(k,0)\} < 23$ (i.e., $|\exp(\Psi(k,0))| < 10^{10}$), and Eqs. (3.2) and (3.5) are used if Re$\{\Psi(k,0)\} \geqslant 23$. It is necessary to select a sufficient number of radial integration points N, to adequately sample the rapid radial oscillations of the TG waves. It was found that the fractional error in the calculated resistance $(R_A - R_P)/R_A$ decreased at the approximate rate $1/N^{1.75}$. For all calculations N was chosen large enough to produce an error less than 1%. The cylinder is assumed to be sufficiently long to sample the narrowest spectral resonance. The calculation is performed using a C-based PC computer program, with a graphical interface, called HE-LIC. It implements the analysis described herein for a wide range of parametrized density profiles and calculates the various power functions and resistances, as well as the electric and magnetic fields and the current as a function of z for
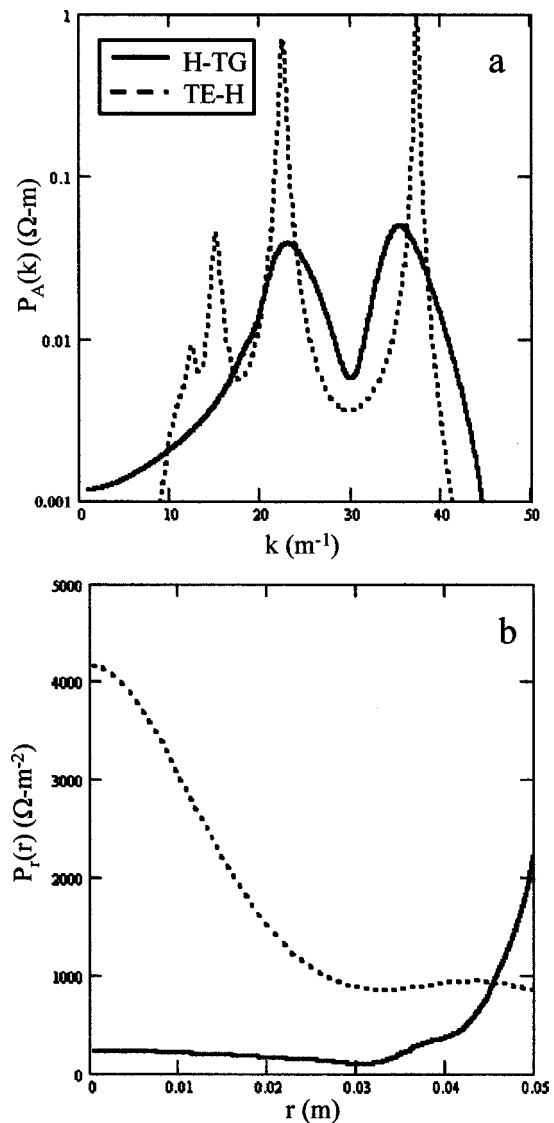
fixed r, and a function of r for fixed z. Simple plots of these functions are also provided. The code is currently being beta tested for later release.

B. Uniform density

Consider first uniform densities for which closed form solutions are available. The power spectral functions and radial absorption profiles for the TE-H and H-TG solutions are shown in Fig. 1 for a plasma density $n_0 = 10^{11}$ cm^{-3} and $B_0 = 25$ G. Even at this low density and magnetic field the TE-H solution absorption profile is more sharply peaked than the analytic one. The respective antenna resistances are 5.67 and 1.39 Ω, a ratio of about 4. Apparently the TE-H approximation yields a larger loading resistance because of the spuriously high peaks in the k spectrum. Both solutions predict peak absorption on axis with the TE-H displaying a larger peak relative to the surface. Figure 2 shows the results for $n_0 = 10^{12}$ cm^{-3} and $B_0 = 100$ G. Both solutions have two dominant resonant modes at approximately the same wave

FIG. 4. H-TG power absorption spectrum as a function of accelerated electron energy $u = \frac{1}{2}m_e(\omega/k)^2$ for $n_0 = 4, 6, 8, 10 \times 10^{12}$ cm^{-3}.
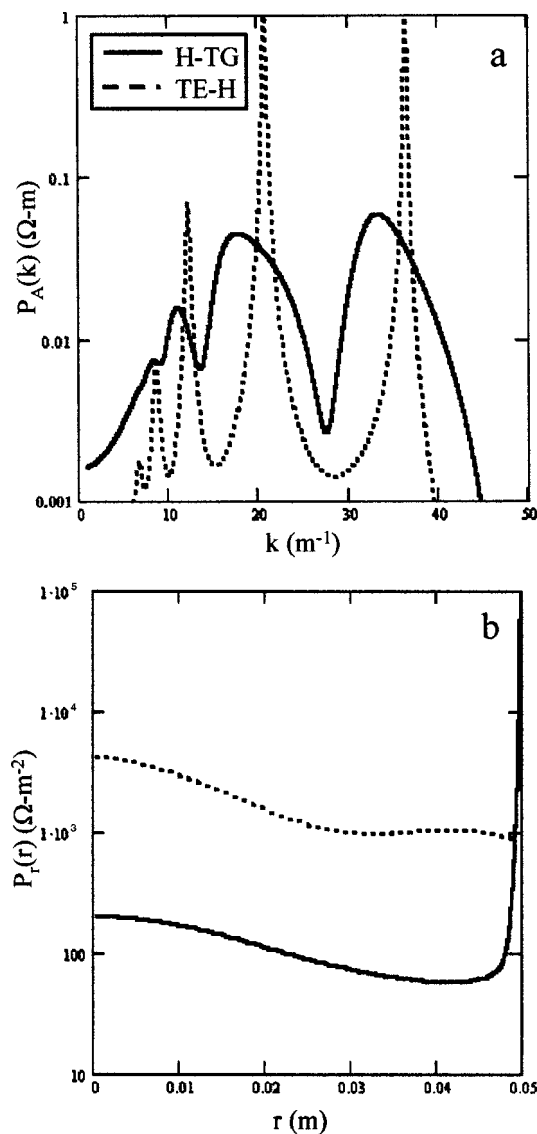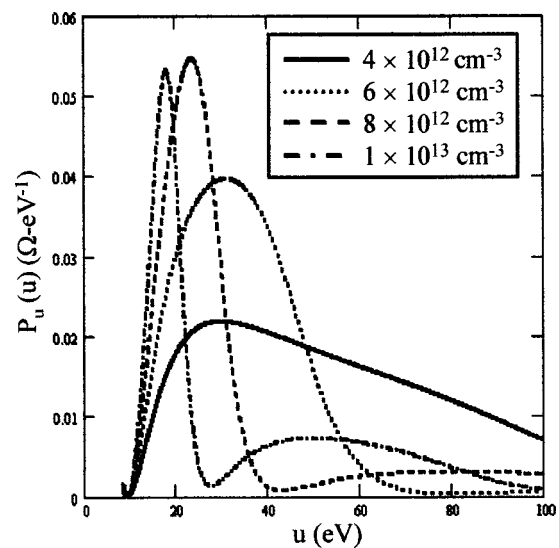

FIG. 3. H-TG vs TE-H power absorption spectrum (a), and radial profile (b), for a uniform density $n_0 = 10^{13}$ cm^{-3} and magnetic field $B_0 = 1000$ G.

number. The TE-H solution displays an additional, lower power, long wavelength mode. The TE-H and H-TG antenna resistances are 2.97 and 1.20 Ω, a reduced ratio of about 2.5. The TE-H peaks have increased and narrowed, but the integrated power has not increased correspondingly. The TE-H absorption still peaks on axis, but has a flat plateau starting about midway to the surface. The H-TG profile peaks on the surface and decreases exponentially radially inward, indicating the dominance of the TG waves in absorption for these parameters. Approximately 75% of the power is deposited in a 1-cm-thick surface layer. The pattern is continued for $n_0 = 10^{13}$ cm^{-3} and $B_0 = 1000$ G, shown in Fig. 3, where the TE-H and H-TG resistances are 3.21 and 1.81 Ω. In that case the width of the TE-H spectral resonances are of the order of 0.2 m^{-1}. In an ideal cavity, where the axial cavity modes are separated by π/L (L is the cavity length), the cavity would have to be 15 m long to ensure that the TE-H modes are excited. Thus, a major result of the broadening of the resonances by the TG modification of the denominators in Eqs.

(2.3) and (3.6) is to permit excitation of the helicon modes in cavities of acceptable length. For plasma stability $\partial R/\partial n_0 \leqslant 0$ at constant B_0 is required.[23] The peak of $R(n_0, B_0)$ for $B_0 = 1000$ G occurs for $n_0 = 4 \times 10^{12}$ cm^{-3}. The H-TG power absorption as a function of accelerated electron energy is shown in Fig. 4 for $n_0 = 4, 6, 8, 10 \times 10^{12}$ cm^{-3}. The curves all diminish rapidly for $u > 100$ eV even for the cases where long wavelength secondary peaks are present, due the factor $u^{-3/2}$ in Eq. (4.3). The corresponding result for the TE-H solution shows large peaks with widths less than about 1 eV. Thus, the H-TG theory predicts that the waves are preferentially absorbed in a broad range of energies from about the ionization threshold up to about 100 eV, depending on the density. This contrasts with the TE-H theory that suggests the presence of electron beams with narrow energy spreads. Calculation of the radial dependence of the wave magnetic field 20 cm from the antenna, $\underline{B}(r,0.2)$, for $n_0 = 10^{12}$ cm^{-3} and $B_0 = 100$ G yielded only small deviations between the H-TG and TE-H solutions. They were located in the 1 cm surface layer. The effect of the broadening on the variation of $\underline{B}_z(0,z)$ for the same parameters is shown in Fig. 5. The magnitude of $\underline{B}_z$ calculated using the TG-H approximation clearly displays a beat phenomenon between the modes and a gradual decay, as seen in experiments.[24] The calculated beating is less pronounced, and the decay is more rapid with the H-TG formulation, due to interference between the wide range of k's in the broadened spectrum shown in Fig. 2. However, as seen in Fig. 5(b), the phase is surprisingly little affected. Since there are many effects not included which can affect the rate of spatial decay, it would be difficult to use the measurement of $\underline{B}_z(0,z)$ to distinguish between the H-TG and TE-H result.

Contour plots of the antenna resistances for the two approaches in the range $10^{12} \leqslant n_0 \leqslant 10^{13}$ cm^{-3} and $100 \leqslant B_0 \leqslant 2000$ G are shown in Fig. 6. The contours of constant R in the TE-H approximation are straight lines (i.e., $B_0 \propto n_0$). The ridge of maximum R (≈ 5.9 Ω) is given approximately by
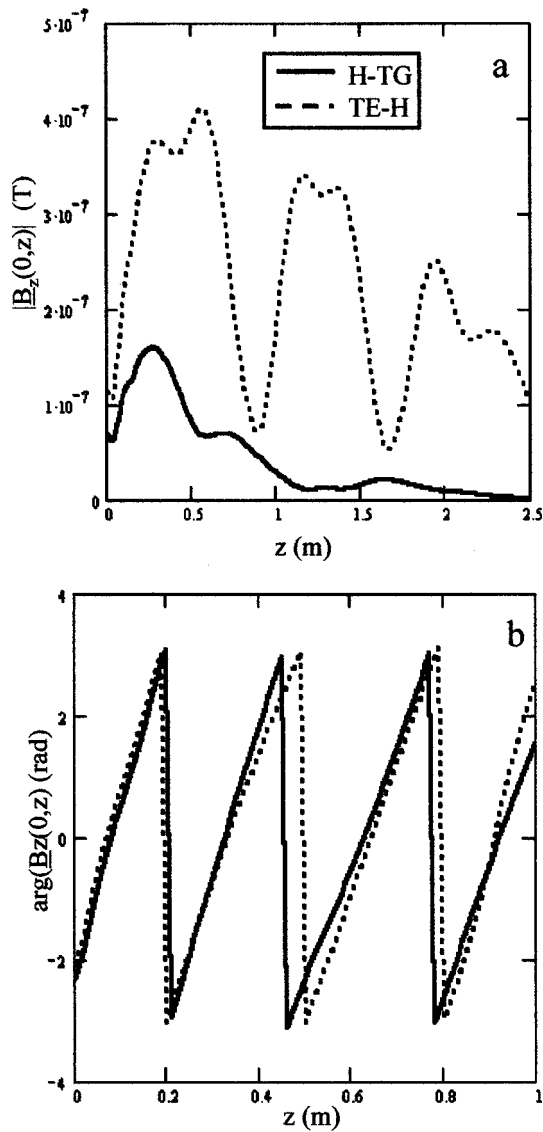
FIG. 5. H-TG vs. TE-H amplitude (a), and phase (b) of the axial wave magnetic field on axis as a function of z, $\underline{B}_z(0,z)$, for a uniform density $n_0 = 10^{12}\,\mathrm{cm}^{-3}$ and magnetic field $B_0 = 100\,\mathrm{G}$.

FIG. 6. Contours of constant H-TG (a), and TE-H (b) antenna resistance (Ω), as a function of density and magnetic field.

$B_0(\mathrm{G}) = 250 \times 10^{-12} n_0(\mathrm{cm}^{-3})$. The local peak resistance of the H-TG contour plot near $n_0 = 2.3 \times 10^{12}\,\mathrm{cm}^{-3}$ and $B_0 = 550\,\mathrm{G}$ is approximately 3.5 Ω. The resistance varies slowly along the ridge, dropping to 2.8 Ω at the saddle point $n_0 = 6.5 \times 10^{12}\,\mathrm{cm}^{-3}$ and $B_0 = 1500\,\mathrm{G}$, and rising to 3.6 Ω at $n_0 = 6 \times 10^{12}\,\mathrm{cm}^{-3}$ and $B_0 = 2000\,\mathrm{G}$. The ratio of resistance calculated using the TE-H and H-TG treatments is in the general range 1.5–2. The ridge in the H-TG contour plot follows approximately a straight line for $B_0 < 1000\,\mathrm{G}$. The line intersects $n_0 = 8 \times 10^{12}\,\mathrm{cm}^{-3}$ at 1500 G. The spectra for $B_0 = 1500\,\mathrm{G}$ and $n_0 = 5, 6.5$, and $8 \times 10^{12}\,\mathrm{cm}^{-3}$ are shown in Fig. 7. The resistances vary slowly (2.7, 2.8, and 2.7 Ω, respectively) although there is significant variation in the spectral shapes.

C. Nonuniform density

It is of interest to explore the effect of the radial density profile on the power absorption. Linear $(1 - r/w)$ and para-
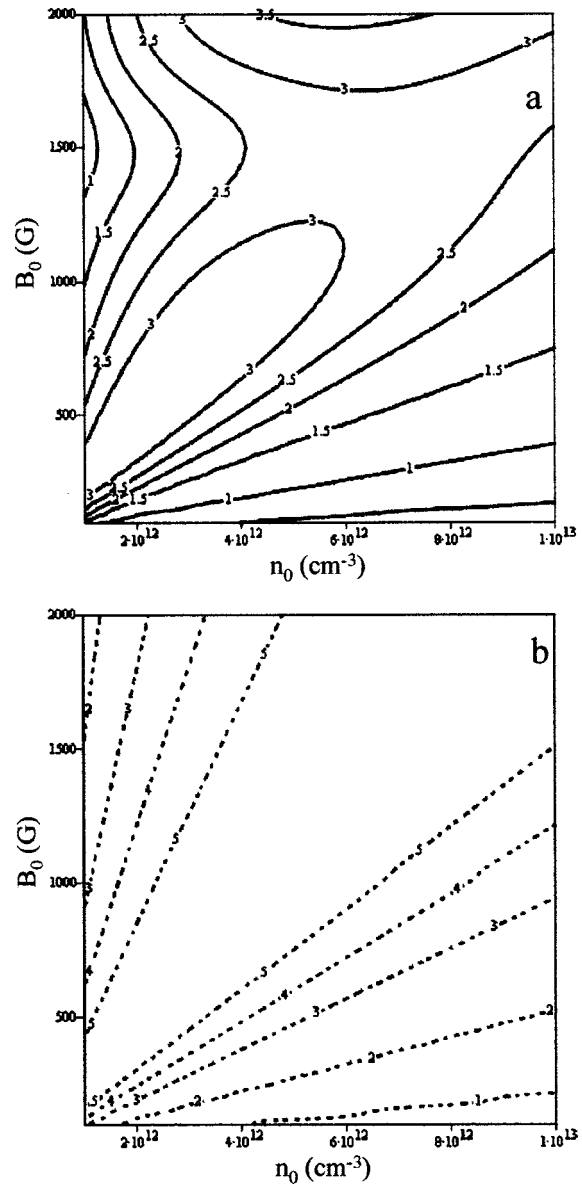
bolic $(1 - (r/w)^2)$ profiles, where w is adjusted to keep the ratio of central to surface density equal 10, were calculated and the results compared to a uniform profile. In the three cases shown in Fig. 8, B_0 is 1000 G and $n_0 = 10^{13}\,\mathrm{cm}^{-3}$ on axis. As the density profile becomes more centrally peaked, the resonances shift to smaller wave number and become narrower, but remain much broader than those predicted by the TE-H approximation. The antenna resistance for the uniform, parabolic, and triangular profiles equal 1.81, 3.17, and 3.36 Ω, respectively. Much greater power dissipation on axis occurs for the centrally peaked profiles. This result is consistent with the experimental observations that density profiles for high power, high-density discharges are centrally peaked[25] and approximately triangular for the highest density cases. The high dissipation on axis sustains the high density there, and the high dissipation near the surface sustains the high power loss to the walls. Calculations were performed
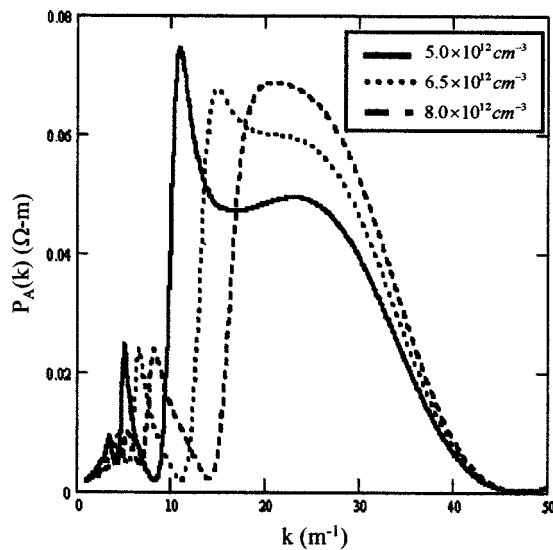
FIG. 7. H-TG power absorption spectrum at $B_0 = 1500$ G and uniform densities $n_0 = 5$, 6.5, and 8×10^{12} cm^{-3}.

using the same profiles but with the central densities increased by a factor of 2 and 3 for the parabolic and triangular shapes so that total amount of plasma was approximately the same for the three cases. The results were similar to those shown in Fig. 8, except that the antenna resistance only increased to about 2.5 Ω for the centrally peaked cases. The diminished enhancement is due to the fact that, at constant magnetic field, the resistance decreases with density in this parameter range.

V. SUMMARY AND CONCLUSIONS

The H-TG solution of the uniform-density, collisional plasma model of antenna coupling was compared to a well-defined, transverse-electric, pure helicon model. For moderate to large static magnetic fields ($B_0 \gtrsim 100$) differences between the configuration-space wave magnetic fields predicted by the two solutions were found to be small and/or difficult to measure. Differences in the spectrum and the radial profile of the power absorption, as well as the topography of the antenna resistance $R(n_0, B_0)$, critical to optimal plasma source design, were found to be significant. The predicted TE-H resistance is typically somewhat less than twice the resistance predicted by the H-TG method. The reduced resistance in the H-TG calculation occurs partly because the presence of TG waves changes the predicted electric fields and currents, but more important because they modify the charge and current balance at the plasma surface and consequently the height and width of the plasma resonance. At large magnetic fields the predicted TE-H resonance is extremely narrow, requiring a very long cavity to ensure overlap between the resonance and the axial cavity modes at equilibrium, as well as in the temporal approach to equilibrium. Landau damping for the H-TG solution is predicted to occur in a broad range of energies from about 10 to about 100 eV, in contrast to the TE-H solution that predicts the presence of narrowly energetic beams. For a uniform density and large magnetic field, both models predict a small axial
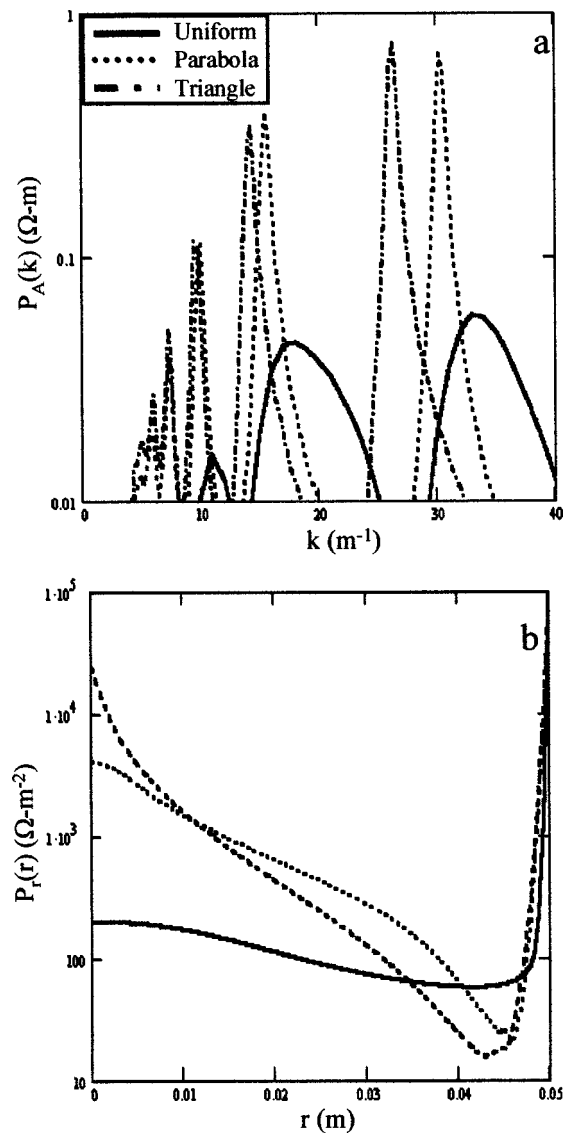

FIG. 8. H-TG power absorption spectrum (a) and radial profile (b) for uniform, parabolic and triangular density profiles. The magnetic field is 1000 G and the density is 10^{13} cm^{-3} on the axis for each case.

peak in the power absorption profile, with the H-TG solution predicting an additional sharp increase in the absorption in a thin surface layer. For more realistic, centrally peaked, density profiles the H-TG solution predicts a thickening of the surface layer as well as a much more pronounced peak in the heating on the axis.

ACKNOWLEDGMENTS

[1] M. A. Lieberman and R. A. Gottscho, in *Physics of Thin Films* (Academic, New York, 1994).
[2] F. F. Chen, Phys. Plasmas **3**, 1783 (1996).
[3] J. P. Klozenberg, B. McNamara, and P. C. Thonemann, J. Fluid Mech. **21**, 545 (1965).
[4] H. A. Bleven, P. J. Christiansen, and B. Davies, Phys. Rev. Lett. **28**, 230 (1968).

[5] R. W. Boswell, Aust. J. Phys. **25**, 403 (1972).

[6] R. W. Boswell, J. Plasma Phys. **31**, 197 (1984).

[7] F. F. Chen, Plasma Phys. Controlled Fusion **33**, 339 (1991).

[8] I. D. Sudit and F. F. Chen, Plasma Sources Sci. Technol. **5**, 43 (1996).

[9] A. R. Ellingboe and R. W. Boswell, Phys. Plasmas **3**, 2797 (1996).

[10] A. Komori, T. Shoji, K. Miyamoto, J. Kawai, and Y. Kawai, Phys. Fluids B **3**, 893 (1991).

[11] S. Shinohara, Y. Miyauchi, and Y. Kawai, Plasma Phys. Controlled Fusion **37**, 1015 (1995).

[12] K. P. Shamrai and V. B. Sharanov, Plasma Phys. Controlled Fusion **36**, 1719 (1994).

[13] K. P. Shamrai and V. B. Sharanov, Plasma Sources Sci. Technol. **5**, 474 (1996).

[14] I. D. Sudit and F. F. Chen, Plasma Sources Sci. Technol. **5**, 43 (1996).

[15] I. V. Kamenski and G. G. Borg, Phys. Plasmas **3**, 4396 (1996).

[16] F. F. Chen and D. Arnush, Phys. Plasmas **4**, 3411 (1997).

[17] D. Arnush and F. F. Chen, Phys. Plasmas **5**, 1239 (1998).

[18] G. G. Borg and R. W. Boswell, Phys. Plasmas **5**, 564 (1998).

[19] T. H. Stix, *Theory of Plasma Waves* (McGraw–Hill, New York, 1962).

[20] K. P. Shamrai and V. B. Taranov, Phys. Lett. A **204**, 139 (1995).

[21] G. N. Haddad and T. F. O'Malley, Aust. J. Phys. **35**, 35 (1982).

[22] G. N. Watson, *A Treatise on the Theory of Bessel Functions* (Cambridge University Press, Cambridge, 1966).

[23] K. P. Shamrai, Plasma Sources Sci. Technol. **7**, 499 (1998).

[24] M. Light, I. D. Sudit, F. F. Chen, and D. Arnush, Phys. Plasmas **2**, 4094 (1995).

[25] D. G. Miljak and F. F. Chen, Plasma Sources Sci. Technol. **7**, 61 (1998).